A study on soil moisture under different land management practices across two rural municipalities in semi-arid region of Mustang, Nepal

S. Dhakal[1] *, S. Kandel[1], & R. Subedi[2]

Received: 03, May 2024 Revised: 11, August 2024 Accepted: 28, August 2024 Published: 22, November 2024

Soil moisture refers to the water amount present in the soil, which is a critical factor influencing plant growth, nutrient cycling, and groundwater recharge. Accurate information on soil moisture-level is crucial for water resource management, agriculture, land degradation, and ecosystem health assessment in semi-arid mountainous regions. Therefore, this study aims to assess average soil moisture under different land managements of the two rural municipalities (Thasang and Gharapjhong) of the Mustang Valley using remote sensing and a geospatial approach. Sentinel-1 and Sentinel-2 data were processed in Google Earth Engine to derive soil moisture using the modified Dubois and Topp's models. The key findings demonstrated that the spatial distribution of soil moisture ranged from 0.01 to 0.4 m^3/m^3 with cropland exhibiting the highest values (0.36 m^3/m^3). The correlation of the average soil moisture with the rainfall showed a strong positive correlation with the coefficient of determination (R^2) of 0.94. The findings of this paper contributes for a better understanding of soil moisture dynamics of different land cover types of this study region. Further, research on the modeling of soil moisture based on *in-situ* field data and other influencing factors is recommended.

Keywords: GIS, geospatial technique, modified dubois model, topp's model, soil moisture index, surface soil moisture

Soil moisture is the water that is temporarily stored in a shallow layer of the earth's top surface (Gao & Shao, 2012). Soil moisture is a crucial factor in the global energy, water, and carbon cycle, and also plays a significant role in several Earth sciences, such as hydrology, meteorology, climatology, and agronomy (Seneviratne *et al*., 2010). Soil moisture content is important for plant growth and development (Janani & Rajeswari, 2022). For an effective implementation of irrigated agriculture, surface soil moisture (SSM) determination is crucial, particularly in arid or semi-arid locations where crop development and yield may be negatively impacted by water scarcity and poor water quality. Soil moisture aids in hydrological modeling (Brocca *et al*., 2011), overland flow prediction (Brocca *et al*., 2010), numerical weather prediction (Dharssi *et al*., 2011), groundwater potentiality assessment (Dhakal *et al*., 2024), impact assessment of climate on agriculture (Talchabhadel *et al*., 2019), and drought monitoring (Nepal *et al*., 2021). Climate change and its effects have great effects on mountainous environments regarding soil moisture availability (Buytaert *et al*., 2011). This crucial problem of soil moisture measurement has received less attention as a key research area. The knowledge of the variation of soil moisture in diverse land cover had to be assessed to understand the overall scenario and implication of appropriate management practices. Therefore, for environmental preservation, it is essential to accurately and continuously monitor soil moisture

1 Tribhuvan University, Institute of Forestry, Pokhara Campus, Pokhara, Nepal., *E-mail: dhakalsandesh33@gmail.com
2 Arthur Temple College of Forestry and Agriculture, Stephen F. Austin State University, Nacogdoches, TX 75962, USA.

over different land cover types.

Soil Moisture was assessed in two ways- one through the in-situ method and the next through Remote Sensing (RS) methods. *In-situ* measurement provides the most accurate soil moisture measurement; however, it is an extremely tedious process and is expensive and time-consuming (Taktikou *et al*., 2016). The *in-situ* method works for a brief period in a constrained region (Saha *et al*., 2018). So, it is not optimal for rapid and continuous soil moisture monitoring at regional-scale. For SM estimation of the large spatial extent, RS methods are best because of their large coverage, continuous, and easily available data. There were primed available SSM data types, such as Soil Moisture and Ocean Salinity (SMOS) and Soil Moisture Active Passive (SMAP) for numerous applications (Brown *et al*., 2013; Kerr *et al*., 2010; Tiwari *et al*., 2023). These products, however, were not appropriate for minor regional planning at landsape-level due to their coarser spatial resolution (about 10 km). To recover SSM at a finer scale, several researches based on Synthetic Aperture Radar (SAR) have been introduced (Mirsoleimani *et al*., 2019; Yadav *et al*., 2020). It proved challenging to extract SSM using SAR data in the presence of vegetation (i.e., sparse and dense cover) because of volume scattering, leaf moisture content, and underlying soil surface scattering (Petropoulos *et al*., 2020).

SAR-based X, C, L, and P-bands have been used in several investigations in the past to recover surface soil moisture over a variety of land cover types, including bare ground, agricultural fields, and surfaces with sparse vegetation (Bhogapurapu *et al*., 2022; Hajj *et al*., 2016; Parida *et al*., 2022; Shen *et al*., 2020). Though the penetrating powers of the L-band make it the most useful of these bands (Ottinger & Kuenzer, 2020), L-band was typically not easily available due to the restricted number of sensors and their wholistic coverage, which was not offered for free, and easy data availability. Consequently, as a result, various research was conducted after the applicability of the Sentinel-1A (C-band) satellite to collect SSM and use the information to water management procedures including scheduling irrigation (Le page *et al*., 2020) and monitoring agricultural development (Hajj *et al*., 2017). This was because the backscattering of radar signals for SSM depended on the incidence angle in addition to SAR bands and the sensitivity of radar signals was stronger at lower incidence angles (Hosseini *et al*., 2015). The radar backscattering coefficient was also influenced by a few other target factors, such as terrain, plant cover, soil types, surface roughness, and dielectric constant (Pasolli *et al*., 2014). The radar backscattering coefficient (σ°), which rises with the increase in the SSM, was highly influenced by the soil's dielectric constant (Xing *et al*., 2019).

Over the years, numerous backscattering models such as physical, empirical, and semi-empirical have been developed. The Water Cloud Model (WCM) was typically employed on vegetated areas that range from sparse to dense. The radar signal was modeled by WCM as a combination of vegetation and soil contributions, attenuated by the vegetation cover and the subsurface (Wang *et al*., 2021). The WCM model uses horizontal-horizontal (HH) or vertical-vertical (VV) polarization to simulate the backscattering coefficient as a function of soil properties (such as soil moisture and surface roughness) and vegetation descriptors, such as plant height, leaf area index (LAI), vegetation water content, and normalized difference vegetation index (NDVI)) (Dong *et al*., 2023). Additionally, SSM was retrieved for several crops using machine learning techniques, such as support vector machine (SVM), random forest (RF), and neural networks (Adab *et al*., 2020; Prakash *et al*., 2018). Most of the researches showed that VV polarization was more sensitive to surface roughness and was superior to vertical-horizontal (VH) polarization for simulating SSM using *in-situ* observations (Yang *et al*., 2023). In addition, Bayesian Merging Method (Wu *et al*., 2017) and change detection process (Zhu *et al*., 2022) have been wisely used to estimate SSM which integrates SAR and passive microwave data. Additionally, with single polarization (VV, HH) SAR data, Nagaraju *et al*., (2013) investigated that the Modified Dubois Model performed more accurately for soil moisture estimation. Singh *et al*., (2020) employed a similar method to obtain

SSM in central India. According to Ji *et al.* (1996), the Dubois Model's ability to recover soil moisture outperformed other models including the "Oh Model". The Dubois Model has the benefit of being able to function on terrain with minimal vegetation and tolerating an NDVI of up to 0.4 (Parida *et al.*, 2022).

The launch of the Sentinel-1A (C-band) and Sentinel-2 satellites and their implications have facilitated many researchers to recover SSM in operations like scheduling irrigation and monitoring crop growth (Mirsoleimani *et al.*, 2019; Yadav *et al.*, 2020). The Modified Dubois Model and the integrated Topp's Model proved to be appropriate methods for assessing soil moisture with better accuracy. Therefore, this study aims to assess the average soil moisture (from 2015 to 2022) of the Mustang Valley, a semi-arid region, using the Modified Dubois Model and the Topp's Model on the Google Earth Engine (GEE) platform. Similarly, the accuracy of the retrieved soil moisture map was performed using the valid spring source locations and stream features over the study area. Finally, the variation of soil moisture contents in different land covers were also assessed. The findings of this study are expected to contribute to a better understanding of soil moisture dynamics within the study area.

Materials and methods

Study area

The study was conducted in the rural municipalities of Thasang and Gharapjhong within Mustang District, Gandaki Province, western Nepal (see Figure 1). This area covers 577.97 sq km and has a population of 6568 (CBSC, 2021). It is located between 28° 33'–28° 52' N latitudes and 83° 28' 30"–83° 53' E longitudes. The elevation of the terrain ranges from 1,372 m to 2863 m above the

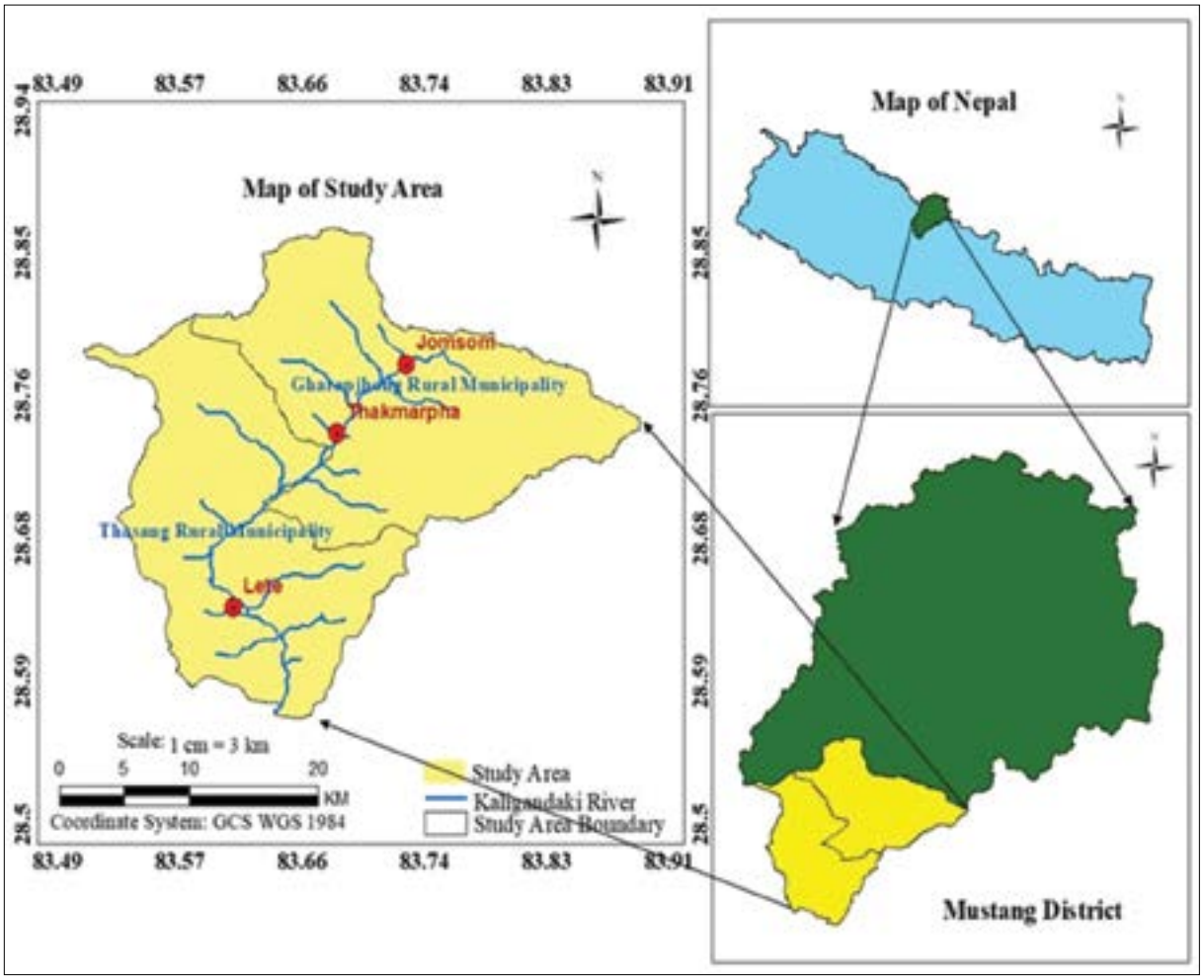

Figure 1: Location of the study area in the map of Nepal.

mean sea level (msl); the terrain is featured with elevated mountains, river valleys, spurs, saddles, vividly colored stratified rock formations, barren high-altitude semi-arid areas, and ridges. The study area encompasses the Kali Gandaki River flowing through its center. This region is a prime example of the Trans-Himalayan zone, with its characteristic continental climate and extreme temperature swings. It is also vulnerable to climate change (Giri, 2017), and its impact such as precipitation of higher snowfall together with rapid melting may favor the occurrence of flash floods (Fort, 2015). The area is protected from monsoon impacts as it is situated on the drier side. Typically, it receives an average annual rainfall of 1097 mm, most occurring durung summer and least during winter. In 2022, the annual precipitation at Lete (situated between 28° 37′ 57.83"–28°37′12″ N latitudes and 83° 36′ 33.19″–83°36′0″ E longitudes at 2490 m above the msl) was around 1813 mm (DHM, 2022). In the same year, the annual precipitation was found to have decreased to below 531mm at Thakmarpha (situated between 28° 44′ 27.27″– 28°47′24″ N latitudes and 83° 40′ 53.81″–83.68′ 00.0″ E longitudes at 2,695 m above the msl) and further to below 300 mm at Jomosom (situated between 28° 47′ 2.43″–28°47′0″ N latitudes and 83° 43′ 47.34″–83°43′50″ E longitudes at 2,740 m above the msl). At elevations above 2,500 m above the msl, most of the snowfall happens during winter although unusually heavy snowfall can occur throughout the year (Khadka *et al*., 2020). This study has generated baseline data for decision-makers to understand the SSM and the sustainable management of resources within the aforementioned two rural municipalities. The study was accomplished in 2023.

Models used for soil moisture estimation

The launch of the Sentinel-1A Satellite in April 2014 improved the availability as well as the spatial and temporal-resolution SAR data for use in estimating soil moisture around the world (Wagner *et al*., 2009). The Sentinel-1A Satellite Sensor collects data on the earth's surface in selectable single (HH or VV) and dual polarization (HH + HV, VV + VH) modes while operating in the C-band at a frequency of 5.405 GHz (Bauer-Marschallinger *et al*., 2018). Table 1 below enlists several techniques and models for soil moisture estimation using sentinel-1 C-Band data; among those, we chose the Modified Dubois Model and Topp's Model for soil moisture retrieval. The Dubois Model is easy to implement and it performs well in steep terrain. Besides, it accounts for surface roughness which is a critical factor in mountainous regions (Thanabalan *et al*., 2018). On the other hand, the Topp's Model is not directly affected by terrain as it operates on dielectric constant data (Ma *et al*., 2021).

Table 1: Techniques used to retrieve soil moisture using Sentinel-1 C-Band GRD data

S. N.	Models	Indices used to retrieve soil moisture	Data used	Polarization or bands	Suitability
1.	Water Cloud Model (WCM)	RVI NDVI, LAI	Sentinel-1 Sentinel-2	VV, VH, HH, HV B4, B8	Densely vegetated areas
2.	Machine learning (support vector regression)	SEPAL platform	Sentinel-1	Both single and dual-polarization	Highly uncertain in densely forested areas
3.	Integrated Equation Model (IEM)	LAI, VWC, NDVI, EVI	Sentinel-1 Sentinel-2	VV, VH, HH, HV B4, B8	Both dense and sparsely vegetated areas
4.	Bayesian approach	Training data	Sentinel-1 (C & L Bands)	VV, VH, HH, HV	Dense vegetation, bare soil, and agricultural lands
5.	Oh Model	Backscattering coefficient	Sentinel-1	VV, VH, HH, HV	Not applicable over the area with significant vegetation

S. N.	Models	Indices used to retrieve soil moisture	Data used	Polarization or bands	Suitability
6.	Artificial Neural Network (AAN) Approach	Training data, Soil water content, Land surface temperature NDVI	Sentinel-1 Sentinel-2	Dual polarization (VH, HV) B4, B8	Site-specific, precise for agriculture area, and sparsely vegetated areas
7.	Change Detection Approach	Backscattering coefficient, NDVI, Calibration	Sentinel-1	VV, HH, VV/VH	Diverse regions such as agriculture, forest, arid and semi-arid regions, wetlands, and others.
8.	Modified Dubois and Topp's models	Relative soil permittivity, Surface roughness NDVI	Sentinel-1 Sentinel-2	VV B4, B8	Sparsely vegetated areas and bare lands (site-specific)

Data collection

Sentinel-1 and Sentinel-2 Satellite data sources were used to retrieve the soil moisture map. The accuracy assessment of the retrieved soil moisture map was performed using perennial spring source locations and stream features taken via field survey. Similarly, the Google Earth Engine platform was used for soil moisture mapping (Gorelick *et al*., 2017).

Satellite data and GEE

This study aimed to produce the soil moisture map of the study area using Sentinel-1 and Sentinel-2 imageries of 10 m spatial resolution. The Sentinel Imagery on the GEE platform was used in this study. The modified Dubois and Topp's models were used to classify the Sentinel imageries on the GEE cloud computing platform to develop an average surface soil moisture map of the aforementioned two rural municipalities (Thasang and Gharapjhong rural municipalities). Sentinel-1 SAR GRD image provides C-Band SAR data at different modes. We used 709 S1 images and derived an average of an interferometric wide-swath (IW) mode image of January, 2015 to December, 2022, which was in VV polarization with an incidence angle Θ (value ranging from 38^0 to 45^0) to derive the average soil moisture index map of the study area. The Sentinel-1 Image on the GEE platform is already preprocessed with radiometric calibration, speckle noise removal, and terrain correction. Similar to this, 940 Sentinel-2 MSI images were chosen for detecting the mean pixel value; the imageries were processed using the red (R) and near-infrared (NIR) bands to get the average NDVI over the period. Table 2 shows the characteristics of the multi-temporal Sentinel data used for the purpose of the study.

Table 2: Characteristics of multi-temporal Sentinel data used in the study

Region of interest	Image series	Date	Season	Band	Total no. of bands used in data cubes
Thasang and Gharapjhong rural municipalities, Mustang district	Sentinel-1 GRD Sentinel-2	January, 2015 to December, 2022	All-season	VV Red and NIR	1 2

Location of spring sources

The field campaign was conducted (during 20–27 April, 2023) to locate the sources of the perennial spring sources with the help of GPS and a participatory-based approach. The spring sources that could not be accessed for direct observation due to difficult geographical terrain were located with the help of a participatory approach. A total of twenty-nine spring sources were located within the study area. The information on the perennial spring sources were used for assessing the accuracy of the derived SSM map based on the assumption that "springs play a role in maintaining soil moisture". Figure 2 below shows the spatial distribution of spring source locations within the study area:

Rainfall data

The Department of Hydrology and Meteorology in Gandaki Province, Pokhara provided the precipitation data from January, 2015 to December, 2022, which formed the basis for constructing the average rainfall data of the study area on monthly basis. There were three meteorological stations within the study area- at Lete, at Marpha, and at Jomsom at the elevations of 2490 m, 2655 m, and 2741 m, respectively. The monthly precipitation data from January 2015 to December 2022 was analyzed to determine the average monthly rainfall and its relationship to soil moisture variation**.**

Land Use Land Cover (LULC) data

Landsat-8 or Sentinel-2 data were used by many researchers for land use land cover mapping of their study areas (Dhakal *et al*., 2022; Xiao *et al*., 2022). On the contrary, we used the FRTC-prepared Landsat-based LULC map of Nepal, published in 2022 (https://frtc.gov.np/uploads/files/Study%20Report%20Inner-final.pdf). The FRTC-prepared LULC map includes eleven land cover types- (i) forest, (ii) water bodies, (iii) built-up areas, (iv) grassland, (v) cropland, (vi) other woodland, (vii) bare soil, (viii) bare rock, (ix) river, (x) snow, and (xii) glacier. Out of these, only four land covers, viz. (i) forest (sparse coniferous), (ii) grassland, (iii) cropland, and (iv) bare land were considered for the purpose of our study.

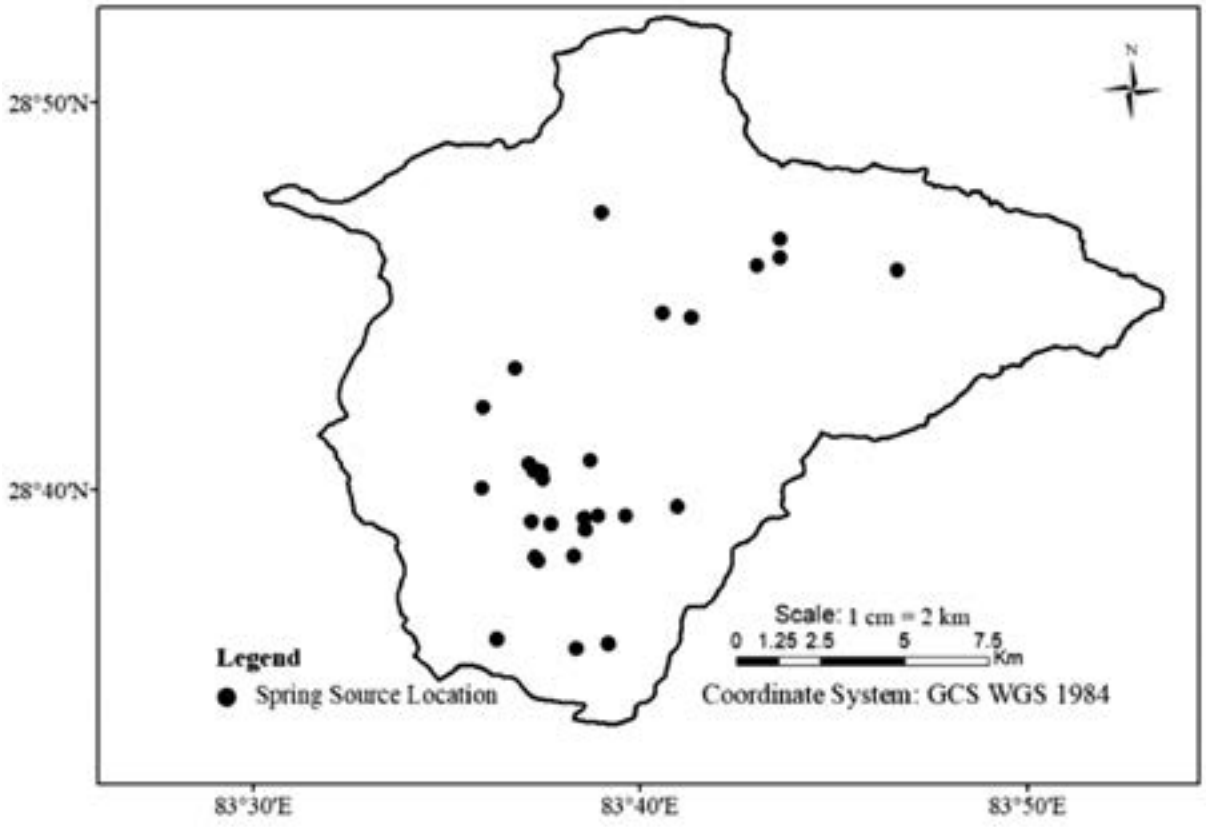

Figure 2: Location of springs within the study area.

Data analysis

Soil moisture index map

The procedure adopted to retrieve the soil moisture is highlighted in Figure 3. In this study, the Modified Dubois Model together with the Topp's Model was used to retrieve the relative soil permittivity using the SAR backscattering values from 'VV' single polarization. The VV polarization band can retrieve soil moisture with greater accuracy as compared to the VH polarization using the Sentinel-1 (Kweon & Oh, 2013). Additionally, the volumetric soil moisture was calculated using the universal Topp's Model and using the relative soil permittivity value. The final map prepared was verified with the help of the valid spring sources and stream features. Figure 3 below depicts the methodology used to estimate the soil moisture:

Sentinel-1 on GEE

In this study, Sentinel-1 images which were already pre-processed and available on the GEE platform were used for data analysis. The images uploaded were of radiometric calibration, speckle noise reduction, and terrain correction. The true backscatter values (σ°) contained in the resultant image pixels were on a linear scale. These values were then transformed to a decibel scale (σ° dB) using the formula:

$$\sigma^\circ \text{ dB} = 10 \times \log10 (\sigma^\circ)$$

The Sentinel-1 Imageries in single polarization (VV) at 10 m x 10 m resolution and the 'IW' instrument mode were used in this study. The incidence angle at this swath varies from 38 to 45 degrees for close and distant ranges, respectively. When paired with Sentinel-1B, Sentinel-1's 12-day temporal resolution was boosted to six days. C-band microwave transmissions may reach a depth of up to 5 cm below the soil's surface (Owe & Van De Griend, 1998).

Sentinel-2 for NDVI on GEE

Sentinel-2 Imagery was used to generate the Normalized Difference Vegetation Index (NDVI) in order to quantify the amount of plant cover in terms of height and density. The NDVI was obtained using the ratio of the difference between Band 8 (Near Infrared) and Band 4 (Red) to the total of Band 8 and Band 4 of Sentinel-2 Images. Nagaraju *et al*. (2013) found that there may be

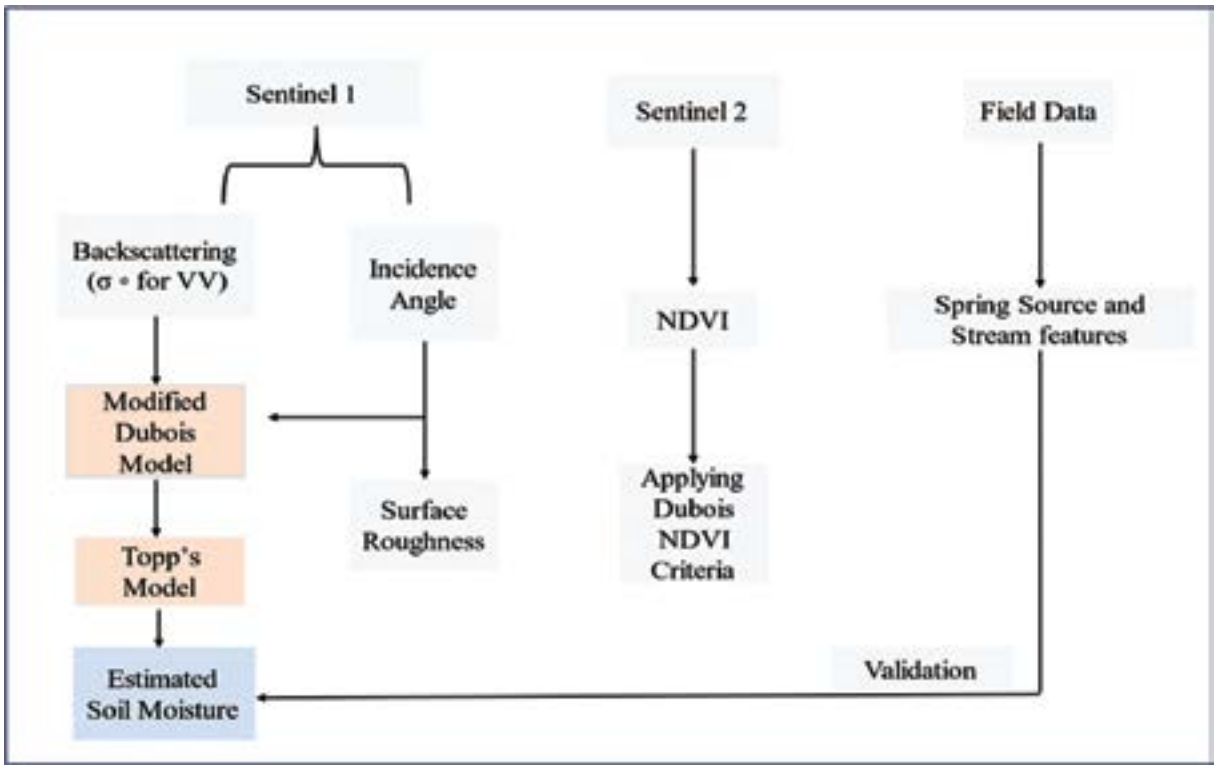

Figure 3: Flow chart depicting the methodology used to estimate soil moisture.

misvalued in regions having NDVI greater than 0.4 while estimating soil moisture using the Modified Dubois Model, which could be due to the limitation of the C-band to penetrate through the dense forest canopy.

Modified Dubois Model

To determine the relative soil permittivity from quad-polarized SAR Images, Dubois *et al*. (1995) devised an empirical model. Originally developed for L, C, and X-band data from scatter meters, this model was later applied to aerial photographs. Even though the portions of the unknown coefficients were obtained by fitting the experimental data, the model structure was developed using compelling physical arguments. Utilizing the backscatter values of VV polarization of the C-band (Sentinel-1A) and incidence angle, the relative soil permittivity (ε) was computed as a Dubois Model Input (Dubois *et al*., 1995). The backscattering coefficient (σ^0) can be calculated using the Equation (1) based on VV polarization:

$$\sigma\circ vv = 10^{-2.37}(\cos^3\Theta/\sin^3\Theta) \times 10^{0.046 \times Extan\Theta} \times (KxSxsin\Theta)^{1.1} \times \lambda^{0.7} \quad \ldots\ldots (1)$$

Where, K stands for $(2\pi/\lambda)$, λ for the SAR wavelength (5.3 cm), S for the soil surface roughness (cm), and Θ for the incidence angle. While the values of Θ and μ were connected to the sensor parameters, the goal parameters, E and S, are often unknown. The Dubois Model was only used in the case of bare soil or sparsely vegetated areas. Therefore, the NDVI of 0.4 criterion is usually applied to retrieve the SSM using the Modified Dubois Model. As per this model, soil permittivity (ε) can be calculated using the Equation (2) based on VV polarization:

$$\text{Soil permittivity } (\varepsilon) = [\log(\sigma\circ vv) - \log(AxC)]/B \quad \ldots\ldots (2)$$

Where, A stands for $10^{-2.37}(\cos^3\Theta/\sin^3\Theta)$, B for 0.046 x tanΘ, and C for $(KxSxsin\Theta)^{1.1}x\lambda^{0.7}$. The unknown surface roughness parameter (S) is assigned as 1.8 cm based on the existing literature on semi-arid regions (Bousbih *et al*., 2018; Singh, *et al.*, 2020; Zribi *et al*., 2014) and we had assumed those regions to be similar to our study area. The study conducted by Bousbih *et al*. (2018) in Kairouan Plain was a semi-arid region typically with agriculture and sparse vegetation cover, and average annual rainfall of approximately 300 mm. Similarly, Zribi *et al.* (2014) claimed that the roughness parameter obtained from their study conducted over the bare soil in the semi-arid region could also be used elsewhere having identical geophysiological conditions. Our study area also possessed similar geographical, climatical, and physiological conditions.

Topp's Model

With the use of the Topp's Model (Thanabalan *et al*., 2022), the volumetric SSM (MV) may be obtained using the Equation (3), where ε was based on the VV polarization of the C-band data (Sentinel–1A). Since this model was not affected by the characteristics of the soil (such as texture or grain size), it was a useful method for simulating surface soil moisture (Song *et al*., 2009).

$$\text{Volumetric SSM (MV)} = -5.3x10^{-2} + 2.92x10^{-2} \times \varepsilon (-5.5)x10^{-4} \times \varepsilon^2 + 4.3x10^{-6} \times \varepsilon^3 \quad \ldots\ldots (3)$$

Validation

Validation was performed using the information on the location of the spring sources and stream features (see Annexes I & II) based on the assumption that "the spring and stream sources play a role in maintaining soil moisture". The linear link between the two variables was measured by buffering the spring and stream features at the distances of <100 m, 100–300 m, and 300–500 m, and the average soil moisture value of this region was analyzed using the zonal statistics (Chen & Hu, 2004; Singla *et al*., 2012). The degree of strength between the soil moisture index value and the distance from the spring and stream sources were used for the validation of the soil moisture map.

Results

Average Soil Moisture Index (SMI)

The existence of plant cover attenuates the soil's contribution, making it more difficult to retrieve

soil moisture from SAR data. The study used an NDVI threshold of 0.4 to identify areas with bare land or sparse vegetation. These areas were excluded from the analysis using the Modified Dubois Model to minimize the influence of vegetation on soil moisture estimation. In the study area, the spatial patterns of the modeled soil moisture revealed that the moisture value ranged from 0.01 to 0.4 m^3/m^3 (Figure 4). The majority of the area had lower soil moisture levels (<0.2 m^3/m^3). A moderate soil moisture level between 0.2 and 0.3 m^3/m^3 was observed across the forest and agricultural areas of the Thasang and Marpha regions. Only the stream sections of the Kali Gandaki River and its tributaries in the eastern, western, and northern parts possessed the maximum soil moisture (0.3–0.4 m^3/m^3).

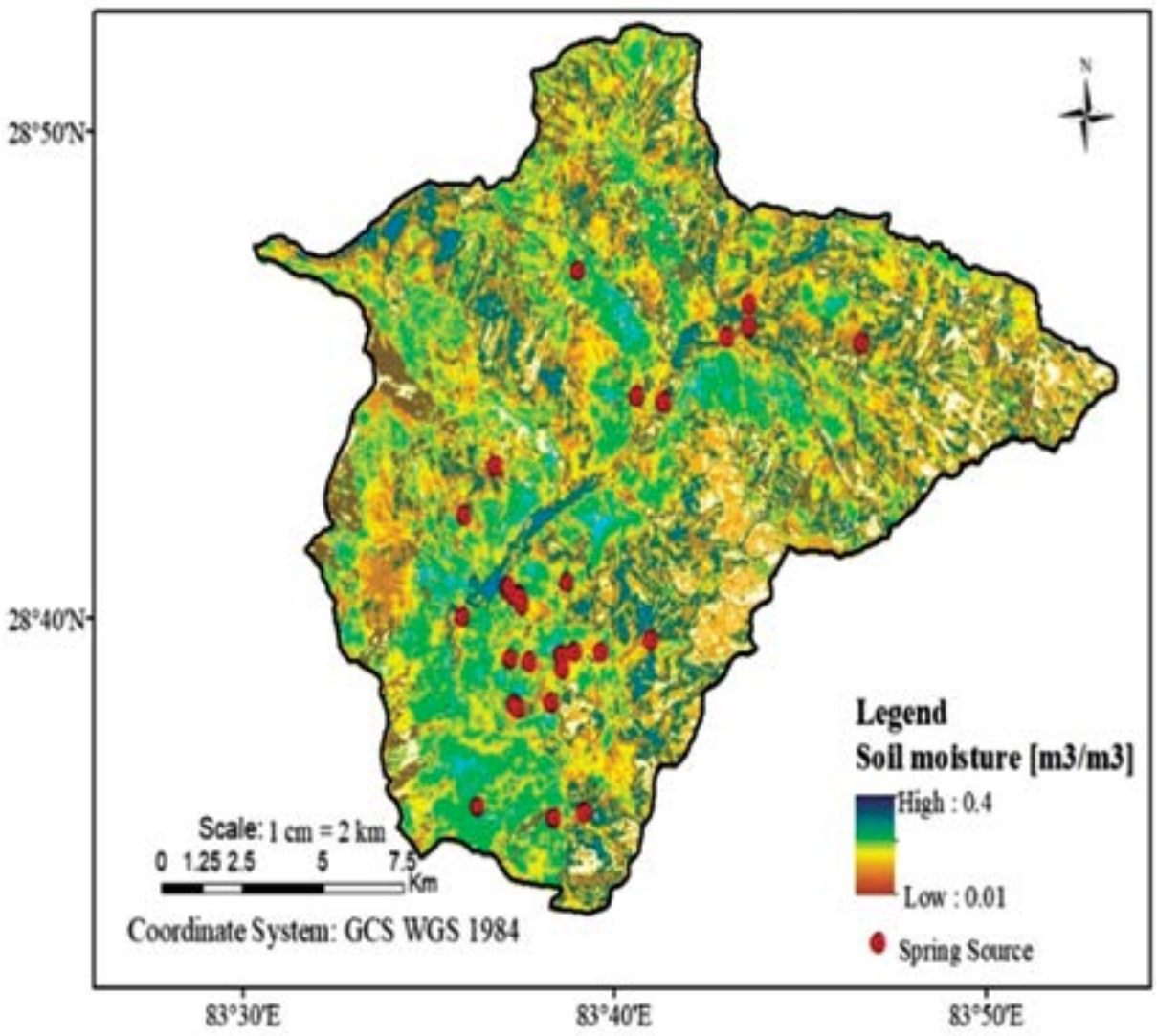

Figure 4: Estimated SSM (m^3/m^3) and its spatial dispersion using Sentinel-1 (*white pixels represent the area outside the scope of the Modified Dubois Model*).

Figure 5 shows the NDVI map of the study area derived from Sentinel-2. The NDVI map was classified into five categories, viz. < 0.1, 0.1–0.2, 0.2–0.3, 0.3–0.4, and > 0.4. Out of the total area (577.97 km^2), 25.78% was under less than 0.1 category, 54.36% under 0.1–0.2 category, 17.41% under 0.2–0.3 category, 2.41% under 0.3–0.4 category, and 0.04% above 0.4 category (Table 3).

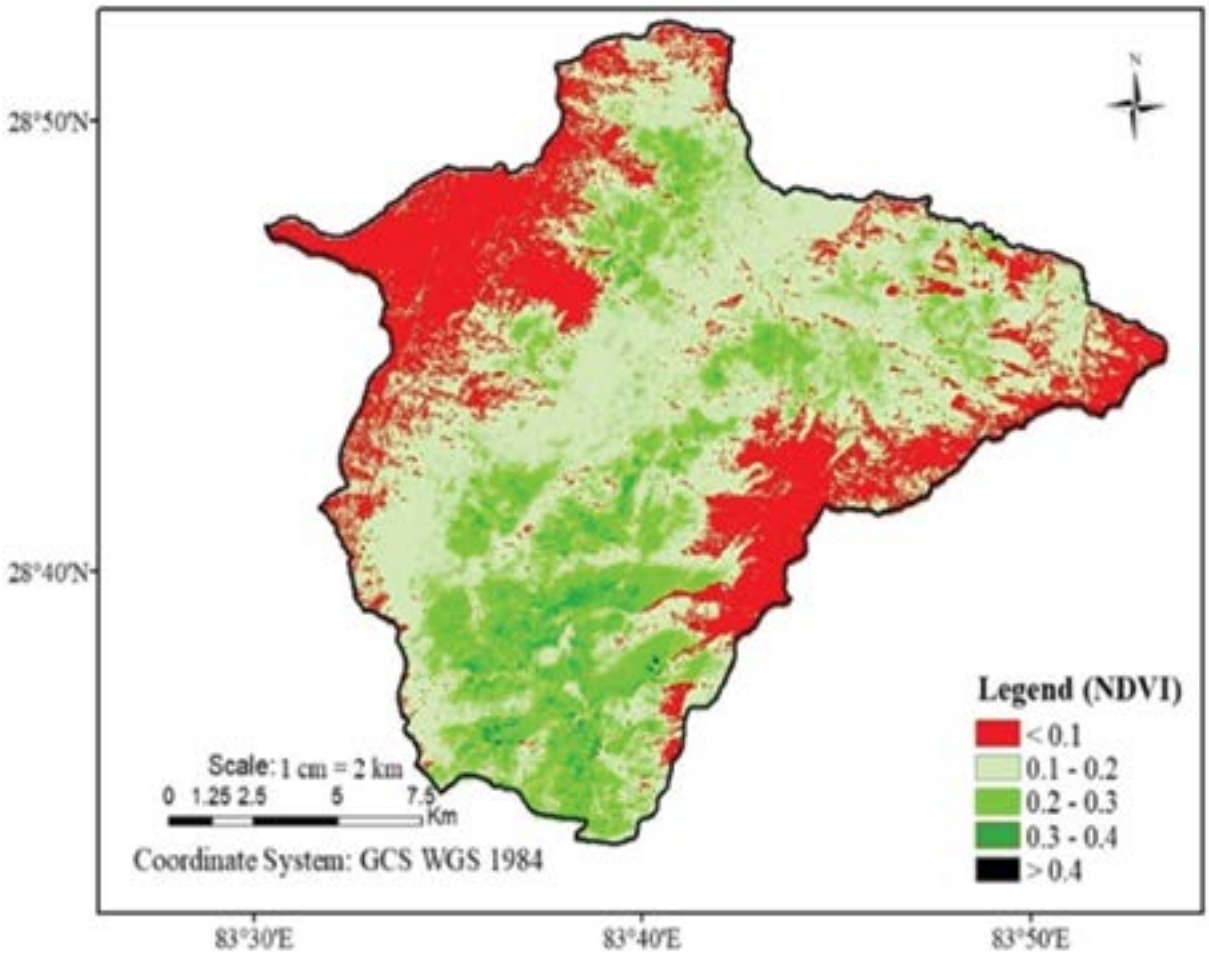

Figure 5: Map showing the NDVI categories of the study area.

Table 3: Percentage coverages of NDVI of the study area

NDVI category	Area (km^2)	Percentage
< 0.1	148.97	25.78
0.1–0.2	314.17	54.36
0.2–0.3	100.62	17.41
0.3–0.4	13.95	2.41
> 0.4	0.25	0.04
Total	**577.97**	**100.00**

Validation

The soil moisture values estimated from Sentinel-1A images were compared with the spring source data and stream features based on the assumption that the closer the region to these water sources higher the soil moisture value. For locations where valid spring and stream sources existed, the corresponding pixels from the modeled soil moisture maps at a distance of <100m, 100 m-300 m, and 300 m-500 m were extracted (Figure 6).

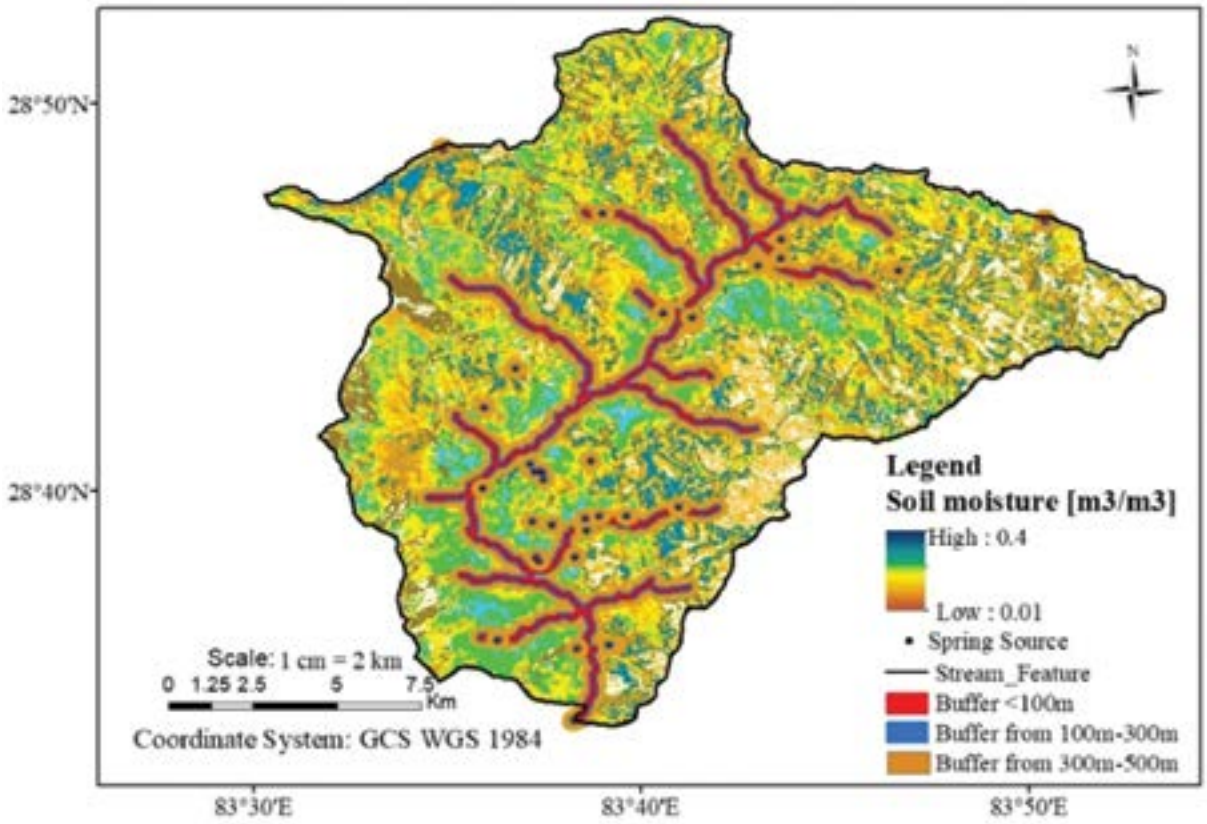

Figure 6: Average soil moisture vs. proximity to spring and stream buffer.

The average soil moisture index (SMI) value was calculated within the distance from the spring and stream source to measure the overall accuracy of the soil moisture map. Table 4 shows the accuracy assessment result that the average SMI value within 100 m was found to be 0.27 (m^3/m^3), 100m-300m was found to be 0.21 (m^3/m^3), and 300m-500m was found to be 0.17 (m^3/m^3) (Annex-1). The accuracy assessment result showed that the retrieved soil moisture map relatively represents a spatial variation of surface soil moisture over the study area.

Table 4: Average soil moisture vs. proximity to stream/spring buffer

Proximity from spring/stream (m)	Percentage coverage area	Av. soil moisture (m^3/m^3)
<100	0.97	0.27
100–300	2.85	0.21
300–500	5.06	0.17
Total	**8.88**	

Analysis of SMI and rainfall across the study area monthly basis

For this analysis, the average soil moisture index from 2015 to 2022 on a monthly basis was plotted in the graph with rainfall data (Figure 7). Here, the monthly average soil moisture in percentage and monthly rainfall in mm were kept on the y-axis and time period (month) on the x-axis.

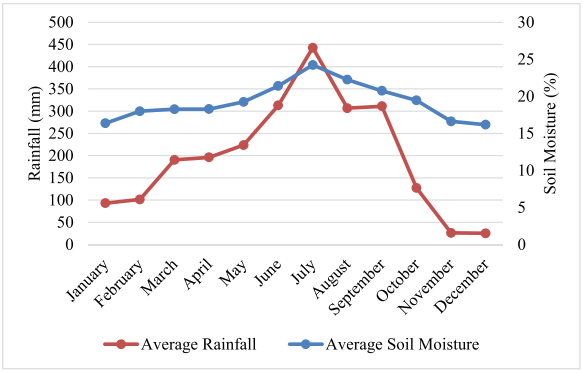

Figure 7: Av. soil moisture vs. av. monthly precipitation during 2015–2022.

The above Chart (Figure 7) represents the change in soil moisture (percentage) vs. monthly precipitation (mm) from January 2015 to December 2022. The average soil moisture was found to be maximum in June, July, and August. It might be due to the influence of monsoon rainfall. Moreover, the overall variation of soil moisture showed that the mean soil moisture increased from January to May and remained higher in June, July, and August (could be due to the rainy season) and slowly decreased from September to December (could be be due to dry season). The average variation of soil moisture was found to be within the range of 16.17% (minimum) and 24.23% (maximum) within the study area. Similarly, the coefficient of determination (R^2) between the soil moisture and rainfall was found to be 0.9469, indicating that there was a strong positive correlation between the soil moisture and the amount of rainfall in the study area.

Land Use Land Cover map

Figure 8 shows the land use land cover map, of the study area, consisting of grassland (44.09%) as the major land cover class followed by bare land (14.5%), sparse coniferous forest (11.09%), cropland (2.89%) and other land cover classes were kept under masked area (27.43%), see also Table 5.

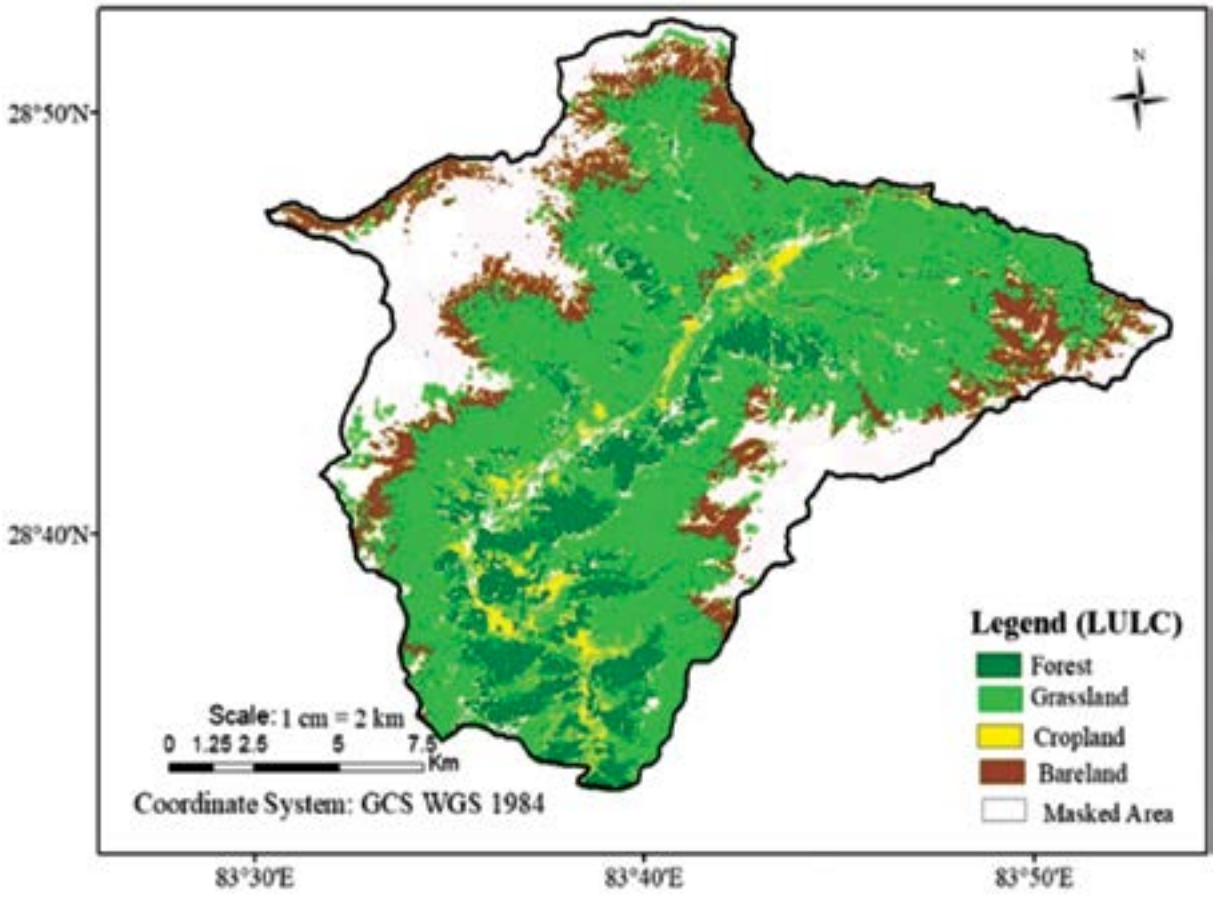

Figure 8: LULC map of the study area.

Table 5: Class-specific LULC of the study area

S. N.	Land Cover	Area (km^2)	Percentage cover
1.	Grassland	254.88	44.09
2.	Bareland	83.81	14.50
3.	Forest	64.15	11.09
4.	Cropland	16.76	2.89
5.	Masked Area	158.37	27.43
Total		**577.97**	**100**

Comparison between average SMI and land cover

The LULC map was derived using the Landsat Imageries with 30 m x 30 m resolution. Therefore, the soil moisture map derived from Sentinel-1 (10 m x 10 m resolution) was resampled into 30 m x 30 m, and then the average pixel value of different land cover types such as forest, cropland, bare land, and grassland was analyzed with the average pixel value for the SMI as shown in Figure 4. The soil moisture in the cropland, and the sparse coniferous forest was found to be somewhat high which was reasonable. The grassland and bareland were found to possess slightly low soil moisture index (value less than 0.2 m^3/m^3, Table 6). This study was based on the SAR data and it was highly dependent on the signal and its reflectance. Different surface types possessed different absorption and reflectance within a pixel; so, the forest and cropland had high soil moisture as the areas vegetation could have overlapped spectral reflectance. Similarly, the soil moisture in cropland was found to be high (0.36 m^3/m^3); the reason for this might be due to the artificial irrigation practiced by the local farmers. Further, the infiltration rate and permeability could play a role in this regard.

Table 6: Average soil moisture with land cover types

S. N.	LULC Features	Soil moisture (m^3/m^3)
1	Cropland	0.36
2	Sparse coniferous forest	0.32
3	Grassland	0.18
4	Bareland	0.12

Discussion

In this study, the VV polarization in the semi-arid zone was used to extract soil moisture based on the Sentinel-1A SAR data using the Dubois Model. The mean surface soil moisture index of the study region from January 2015 to December 2022 was found to have ranged from 0.01 to 0.4 m^3/m^3. The generated soil moisture index gives a first-order approximation of soil moisture despite the limitation of the model's approach, such as their reliance on the frequency of SAR data, the state of the land used, and the types of land cover. The Modified Dubois Model was also used to calculate the soil moisture in the Kosi river basin based on the Sentinel-1 SAR data in north India, and the result showed that the SSM varied from 0.05 m^3/m^3 to 0.5 m^3/m^3 (Parida *et al*., 2022). Additionally, the Modified Dubois Model may be used for the SSM values between 0 and 0.35 m^3/m^3 and the NDVI less than 0.4, which depicts the model's performance declines when moisture level approaches saturation levels (Rao *et al*., 2013). The SSM cannot be obtained using the Modified Dubois Model provided the region has dense vegetation cover (Liu *et al*., 2020; Thanabalan *et al*., 2022). Therefore, the Modified Dubois Model effectively measures SSM, particularly in agricultural areas, areas with bare soil, and semi-arid areas. Alternatively, in areas having dense vegetation cover (NDVI>0.4), the improved water cloud model (WCM) was advised to be applied for deriving SSM (Lei *et al*., 2022; Zribi *et al*., 2019).

Similarly, the variation of soil moisture with different land covers indicated that the SMI of the cropland was found to be highest (0.36 m^3/m^3) followed by forest (0.32 m^3/m^3), grassland (0.18 m^3/m^3), and bareland (0.12 m^3/m^3) which was reasonable as per the findings of the study conducted by Tiwari *et al*. (2023) on SMI of Nepal. Moreover, they also found a positive correlation between vegetation with SMI. The temporal analysis of average soil moisture with rainfall (precipitation) revealed that the SMI correlated with the amount of rainfall, which coincides with the findings of Schoener *et al*. (2020). Several researchers have used SAR data and a variety of models to determine SSM, such as Balenzano *et*

al. (2011), Hajj *et al*. (2016), and Zan & Parizzi (2013). Some studies used ground-based *in-situ* measurement of soil moisture to trend and validate the models, then the obtained soil moisture map was found to correlate well with field scale data, such as Albergel *et al*. (2011) and Rajib *et al*. (2016). The present method can also make it possible to utilize cost-effective remote sensing data for estimating soil moisture for a variety of crop planning and agronomy applications.

Conclusion

Our study exploited VV polarization of the C-band of Sentinel-1A to generate the spatiotemporal pattern of the SSM across the bare soil and minimally vegetated land of the two rural municipalities (Thasang and Gharapjhong) of Mustang district. The spatial variability of soil moisture within the study area was found to have ranged from 0.01 m^3/m^3 to 0.4 m^3/m^3 and has been accurately represented by the suggested technical framework. In course of the analysis of the rainfall data and the SMI figures, the rainfall showed a strong positive correlation with the SMI, with the correlation coefficient of 0.9469. The comparative study on the soil moisture with land cover showed that the SMI of the cropland was found to be the highest (0.36 m^3/m^3) followed by the forest areas (0.32 m^3/m^3). This study contributes toward using remotely sensed data to monitor moisture content of surface soil for tracking the impact of climate change on SSM, crop and water usage, management of water, scheduling crop irrigation, soil erosion, droughts, and flooding with better spatial and temporal resolutions. However, research on modeling SSM based on *in-situ* field data and other influencing factors is essential.

Acknowledgment

We are thankful to the Gandaki Province Academy of Science and Technology (GPAST) for granting us financial support to carry out this study. We are also grateful to Mr. Shambhu Kumar Mishra, Asst. Forest Officer, Divisional Forest & Soil Conservation Office, Kusma, Parbat and the local residents around the study area for helping us during our fieldwork.

Author's contribution statement

Sandesh Dhakal: Conceptualization of the study, development of methodology, data collection, data analysis, and preparation of draft manuscript; **Saroj Kandel:** Investigation of the study, data collection, data analysis, and validation of results; and **Rajan Subedi:** Conceptualization, visualization and supervision of the entire study.

Data availability

The data will be accessible after the request for the data.

Conflict of Interest

The authors declare no conflict of interest.

References

Adab, H., Morbidelli, R., Saltalippi, C., Moradian, M., Abbas, G., & Ghalhari, F. (2020). Machine learning to estimate surface soil moisture from remote sensing data. *Water*, 12 (11): 3223. https://doi.org/10. 3390/w12113223.

Albergel, C., De Rosnay, P., Gruhier, C., Muñoz-Sabater, J., Hasenauer, S., Isaksen, L., Kerr, Y., & Wagner, W. (2011). Evaluation of remotely sensed and modelled soil moisture products using global ground-based in situ observations. *Elsevier*. https://www.sciencedirect.com/science/article/pii/ S0034425711004147.

Balenzano, A., Mattia, F., Satalino, G., Davidson, M., Member, S., Satalino, G., & J Davidson, M. W. (2011). Dense temporal series of C-and L-band SAR data for soil moisture retrieval over agricultural crops. *Ieeexplore.Ieee.Org*, *4* (2): 439. https://doi.org/10.1109/JSTARS.2010.2052916.

Bauer-Marschallinger, B., Freeman, V., Cao, S., Paulik, C., Schaufler, S., Stachl, T., ……., & Wagner, W. (2018). Toward global soil moisture monitoring with Sentinel-1: harnessing assets and overcoming obstacles. *IEEE Transactions on Geoscience and Remote Sensing*, *57* (1): 520–539.

Bhogapurapu, N., Dey, S., Mandal, D., Bhattacharya, A., Karthikeyan, L., McNairn, H., & Rao, Y. S. (2022). Soil moisture retrieval over croplands using dual-pol L-band GRD SAR data. *Remote Sensing of Environment*, *271*: 112900.

Bousbih, S., Zribi, M., El Hajj, M., Baghdadi, N., Lili-Chabaane, Z., Gao, Q., & Fanise, P. (2018). Soil moisture and irrigation mapping in a semi-arid region based on the synergetic use of Sentinel-1 and Sentinel-2 data. *Remote Sensing*, *10* (12): 1953.

Brocca, L., Melone, F., Moramarco, T., Wagner, W., Naeimi, V., Bartalis, Z., & Hasenauer, S. (2010). Improving runoff prediction through the assimilation of the ASCAT soil moisture product. *Hydrology and Earth System Sciences*, *14* (10): 1881–1893. https://doi.org/10.5194/hess-14-1881-2010.

Brocca, L., Moramarco, T., Melone, F., Wagner, W., Hasenauer, S., & Hahn, S. (2011). Assimilation of surface and root-zone ASCAT soil moisture products into rainfall–runoff modeling. *IEEE Transactions on Geoscience and Remote Sensing*, *50* (7): 2542–2555.

Brown, M. E., Escobar, V., Moran, S., Entekhabi, D., O'Neill, P. E., Njoku, E. G., ..., & Entin, J. K. (2013). NASA's soil moisture active passive (SMAP) mission and opportunities for applications users. *Bulletin of the American Meteorological Society*, *94* (8): 1125–1128.

Buytaert, W., Cuesta Camacho, F., & Tobón, C. (2011). Potential impacts of climate change on the environmental services of humid tropical alpine regions. *Global Ecology and Biogeography*, *20* (1): 19–33.

CBSC. (2021). *National Population and Housing Census 2021, Volume 1*. Central Bureau of Stastistics, Thapathali, Kathmandu.

Chen, X. & Hu, Q. (2004). Groundwater influences on soil moisture and surface evaporation. *Journal of Hydrology*, *297* (1–4): 285–300.

Dhakal, S., Kandel, S., Puri, L., & Shrestha, S. (2022). An assessment on land use land cover mapping: Sentinel-2 versus Landsat-9. *Forestry: Journal of Institute of Forestry, Nepal*, *19* (01): 56–63.

Dhakal, Sandesh, Subedi, R., Kandel, S., & Shrestha, S. (2024). Heliyon remote sensing and geospatial approach : optimizing groundwater exploration in semi-arid region, Nepal. *Heliyon*, *10* (10): e31281. https://doi.org/10.1016/j.heliyon.2024.e31281.

Dharssi, I., Bovis, K. J., Macpherson, B., & Jones, D. (2011). Operational assimilation of ASCAT surface soil wetness at the Met Office. *Hydrology and Earth System Sciences*, *15* (8): 2729–2746.

DHM. (2022). *Preliminary Precipitation Summary, Monsoon Season (June–September), 2022*. Department of Hydrology and Meteorology, Babarmahal, Kathmandu.

Dong, L., Wang, W., Jin, R., Xu, F., & Zhang, Y. (2023). Surface soil moisture retrieval on Qinghai-Tibetan Plateau using Sentinel-1 Synthetic aperture radar data and machine learning algorithms. *Remote Sensing*, *15* (1). https://doi.org/10.3390/RS15010153.

Dubois, P., Zyl, J. V., & Engman, T. (1995). Measuring soil moisture with imaging radars. *IEEE Transactions on Geoscience and Remote Sensing*, *33* (4): 915–926.

Fort, M. (2015). Natural hazards versus climate change and their potential impacts in the dry, northern Himalayas: focus on the upper Kali Gandaki (Mustang district, Nepal). *Environmental Earth Sciences*, *73* (2): 801–814. https://doi.org/10.1007/S12665-014-3087-Y.

Gao, L. & Shao, M. (2012). Temporal stability of soil water storage in diverse soil layers. *Catena*, *95*: 24–32.

Giri, M. (2017). Climate change vulnerrability at household-level in urban and rural areas of Nepal. In 8th International Conference on Climate Change [Climate Action: Mitigation, and Adaptation in a

Post Paris World]. 4–5 August, 2017. Centre for Climate Change and Sustainability Studies, Tata Institute of Social Sciences, Mumbai.

Gorelick, N., Hancher, M., Dixon, M., Ilyushchenko, S., Thau, D., & Moore, R. (2017). Google Earth Engine: planetary-scale geospatial analysis for everyone. *Remote Sensing of Environment*, *202*: 18–27.

Hajj, E. M., El Hajj, M., Baghdadi, N., Zribi, M., Belaud, G., Courault, D., & Charron, F. (2016). Soil moisture retrieval over irrigated grassland using X-band SAR data. *Elsevier*, *176*: 202–218. https://doi.org/10.1016/j.rse.2016.01.027.

Hajj, M., Baghdadi, N., Zribi, M., & Bazzi, H. (2017). Synergic use of Sentinel-1 and Sentinel-2 images for operational soil moisture mapping at high spatial resolution over agricultural areas. *Remote Sensing*, *9* (12): 1292.

Hosseini, R., Newlands, N. K., Dean, C. B., Takemura, A., Baghdadi, N., & Thenkabail, P. S. (2015). Statistical modeling of soil moisture, integrating satellite remote-sensing (SAR) and ground-based data. *Mdpi.Com*, *7*: 2753. https://doi.org/10.3390/rs70302752.

Janani, N. & Rajeswari, M. (2022). Effects of organic and inorganic soil conditioners on soil moisture in Ddrylands. *Agropedology*, 32 (02): 219–225. https://doi.org/10.47114/j.agroped.2022.dec7.

Ji, J., van der Keur, P., Thomsen, A., & Skriver, H. (1996, May). Soil moisture retrieval using the Danish L- & C-band polarimetric SAR. In *International Geoscience and Remote Sensing Symposium (IGARSS)*, 1996. 2: 1300–1302. Institute of Electrical and Electronics Engineers (IEEE).

Kerr, Y. H., Waldteufel, P., Wigneron, J. P., Delwart, S., Cabot, F., Boutin, J., ……., & Mecklenburg, S. (2010). The SMOS mission: New tool for monitoring key elements of the global water cycle. Proceedings of the *IEEE*, *98* (5): 666–687.

Khadka, N., Kumar Ghimire, S., Chen, X., Thakuri, S., Hamal, K., Shrestha, D., & Sharma, S. (2020). Dynamics of maximum snow cover area and snow line altitude across Nepal (2003–2018) using improved MODIS data. *Academia, 25* (2): 2467–9240. https://doi.org/10.3126/jist.v25i2.33729.

Kweon, S. K. & Oh, Y. (2013). Estimation of soil moisture and surface roughness from single-polarized radar data for bare soil surface and comparison with dual-and quad-polarization cases. *IEEE Transactions on Geoscience and Remote Sensing*, *52* (7): 4056–4064.

Le page, M., Jarlan, L., El Hajj, M. M., Zribi, M., Baghdadi, N., & Boone, A. (2020). Potential for the detection of irrigation events on maize plots using Sentinel-1 soil moisture products. *Remote Sensing*, *12* (10): 1621.

Lei, J., Yang, W., & Yang, X. (2022). Soil moisture in a vegetation-covered area using the improved water cloud model based on remote sensing. *Journal of the Indian Society of Remote Sensing*, *50* (1). https://doi.org/10.1007/S12524-021-01450-2.

Liu, Y., Qian, J., & Yue, H. (2020). Combined Sentinel-1A with Sentinel-2A to estimate soil moisture in farmland. *IEEE Journal of Selected Topics in Applied Earth Observations and Remote Sensing*, *14*: 1292–1310.

Ma, T., Han, L., & Liu, Q. (2021). Retrieving the soil moisture in bare farmland areas using a modified Dubois Model. *Frontiers in Earth Science*, *9*. https://doi.org/10.3389/FEART.2021.735958/FULL.

Mirsoleimani, H. R., Sahebi, M. R., Baghdadi, N., & El Hajj, M. (2019). Bare soil surface moisture retrieval from Sentinel-1 SAR data based on the calibrated IEM and dubois models using neural networks. *Sensors*, *19* (14): 3209.

Nagaraju, M. S. S., Venugopal, M. V., Rajankar, P., Laghate, P., Reddy, M. S., Joshi, A. K., & Sharma, J. R. (2013). Modified Dubois Model for estimating soil moisture with dual polarized

SAR data. *Journal of Indian Society of Remote Sensing*, *41* (4): 865–872.

Nepal, S., Pradhananga, S., Shrestha, N. K., Kralisch, S., Shrestha, J. P., & Fink, M. (2021). Space–time variability in soil moisture droughts in the Himalayan region. *Hydrology and Earth System Sciences*, *25* (4): 1761–1783.

Ottinger, M. & Kuenzer, C. (2020). Spaceborne L-band synthetic aperture radar data for geoscientific analyses in coastal land applications: a review. *Remote Sensing*, *12* (14): 2228.

Owe, M., & Van De Griend, A. A. (1998). Comparison of soil moisture penetration depths for several bare soils at two microwave frequencies and implications for remote sensing. *Water Resources Research*, *34* (9): 2319–2327. https://doi.org/10.1029/98WR01469.

Parida, B. R., Pandey, A. C., Kumar, R., & Kumar, S. (2022). Surface soil moisture retrieval using Sentinel-1 SAR data for crop planning in Kosi River Basin of North Bihar. *Agronomy*, *12* (5): 1045.

Pasolli, L., Notarnicola, C., Bertoldi, G., Della Chiesa, S., Niedrist, G., Bruzzone, L., ……., & Zebisch, M. (2014). Soil moisture monitoring in mountain areas by using high resolution SAR images: results from a feasibility study. *European Journal of Soil Science*, *65* (6): 852–864.

Petropoulos, G. P., Srivastava, P. K., Ferentinos, K. P., & Hristopoulos, D. (2020). Evaluating the capabilities of optical/TIR imaging sensing systems for quantifying soil water content. *Geocarto International*, *35* (5): 494–511. https://doi.org/10.1080/10106049.2018.1520926.

Prakash, S., Sharma, A., & Sahu, S. S. (2018). Soil moisture prediction using machine learning. IEEE *Xplore.* https://ieeexplore.ieee.org/abstract/document/8473260.

Rajib, M. A., Merwade, V., & Yu, Z. (2016). Multi-objective calibration of a hydrologic model using spatially distributed remotely sensed/*in-situ* soil moisture. *Journal of hydrology*, *536*: 192–207.

Rao, S. S., Sahadevan, D. K., Das, S. N., Nagaraju, M. S. S., Venugopal, M. V., Rajankar, P., …....., & Sharma, J. R. (2013). Modified Dubois Model for estimating soil moisture with dual polarized SAR data. *Journal of the Indian Society of Remote Sensing*, *41*: 865–872.

Saha, A., Patil, M., Goyal, V. C., & Rathore, D. S. (2018). Assessment and impact of soil moisture index in agricultural drought estimation using remote sensing and GIS techniques. Paper presented at the 3rd International Electronic Conference on Water Sciences, 15–30 November, 2018.

Schoener, G., & Stone, M. C. (2020). Monitoring soil moisture at the catchment scale: a novel approach combining antecedent precipitation index and radar-derived rainfall data. *Journal of Hydrology*, *589*: 125–155.

Seneviratne, S. I., Corti, T., Davin, E. L., Hirschi, M., Jaeger, E. B., Lehner, I., ……..., & Teuling, A. J. (2010). Investigating soil moisture–climate interactions in a changing climate: a review. *Earth-Science Reviews*, *99* (3–4), 125–161.

Shen, X., Walker, J. P., Ye, N., Wu, X., Boopathi, N., Yeo, I. Y., ……., & Zhu, L. (2020). Soil moisture retrieval depth of P- & L-band radiometry: predictions and observations. IEEE *Transactions on Geoscience and Remote Sensing*, *59* (8): 6814–6822.

Singh, A., Gaurav, K., & Kumar, S. (2020). Evaluating the potential of Sentinel-1 images for the estimation of soil moisture on an alluvial Fan. In *EGU General Assembly Conference Abstracts* (p. 19614).

Singla, S., Céron, J. P., Martin, E., Regimbeau, F., Déqué, M., Habets, F., & Vidal, J. P. (2012). Predictability of soil moisture and river flows over France for the spring season. *Hydrology and Earth System Sciences*, *16* (1): 201–216.

Song, K., Zhou, X., & Fan, Y. (2009). Empirically adopted IEM for retrieval of soil moisture from radar backscattering coefficients. IEEE *Transactions on Geoscience and Remote*

Sensing, *47* (6): 1662–1672.

Taktikou, E., Bourazanis, G., Papaioannou, G., & Kerkides, P. (2016). Prediction of soil moisture from remote sensing data. *Procedia Engineering*, *162*: 309–316. https://doi.org/10.1016/J. PROENG. 2016.11.066.

Talchabhadel, R., Karki, R., Yadav, M., Maharjan, M., Aryal, A., & Thapa, B. R. (2019). Spatial distribution of soil moisture index across Nepal: a step towards sharing climatic information for agricultural sector. *Theoretical and Applied Climatology*, *137* (3–4): 3089–3102. https://doi. org/10. 1007/S00704-019-02801-3.

Thanabalan, P., & Vidhya, R. (2018). Derivation of soil moisture using modified Dubois Model with field assisted surface roughness on RISAT-1 data. *Earth Sciences Research Journal*, *22* (1): 13–18.

Thanabalan, P., Vidhya, R., & Kankara, R. S. (2022). Soil moisture estimation using RISAT-1 and SENTINEL-1 data using modified Dubois model in comparison with averaged NDVI. *Geocarto International*, *37* (25): 8624–8644.

Tiwari, A., Baniya, B., Dutta, A., KC, P., Gyawali, P., & Ansari, K. (2023). Assessment and prediction of soil moisture index of Nepal using geospatial techniques. https://www.researchgate.net/profile/Amit-Tiwari-40/publication/370591246.

Wagner, W., Sabel, D., Doubkova, M., Bartsch, A., & Pathe, C. (2009). The potential of Sentinel-1 for monitoring soil moisture with a high spatial resolution at global-scale. In *Symposium of Earth Observation and Water Cycle Science*, 3: 60.

Wang, Z., Zhao, T., Qiu, J., Zhao, X., Li, R., & Wang, S. (2021). Microwave-based vegetation descriptors in the parameterization of water cloud model at L-band for soil moisture retrieval over croplands. *GIScience & Remote Sensing*, *58* (1): 48–67.

Wu, X., Walker, J. P., Rüdiger, C., Panciera, R., & Gao, Y. (2017). Medium-resolution soil moisture retrieval using the bayesian merging method. *IEEE Xplore*, *55* (11). Ihttps://doi.org/10.1109/TGRS.2017. 2728808.

Xiao, W., Wu, Q., Li, X., Nasiri, V., Deljouei, A., Moradi, F., Mohammad, S., Sadeghi, M., & Borz, S. A. (2022). Land use and land cover mapping using Sentinel-2, Landsat-8 Satellite Images, and Google Earth Engine: a comparison of two composition methods. Multidisciplinary Digital Publishing Institute (MDPI). https://doi.org/10.3390/ rs14091977.

Xing, M., He, B., Ni, X., Wang, J., An, G., Shang, J., & Huang, X. (2019). Retrieving surface soil moisture over wheat and soybean fields during growing season using modified water cloud model from Radarsat-2 SAR data. *Remote Sensing*, *11* (16): 1956. https://www.mdpi.com/2072-4292/11/16/1956.

Yadav, V. P., Prasad, R., Bala, R., & Vishwakarma, A. K. (2020). An improved inversion algorithm for spatio-temporal retrieval of soil moisture through modified water cloud model using C-band Sentinel-1A SAR data. *Computers and Electronics in Agriculture*, *173*: 105447. https://www.sciencedirect. com/science/article/pii/S0168169919326481.

Yang, H., Song, J., Teng, Y., Song, X., Zeng, P., & Jia, J. (2023). Coupling model-driven and data-driven methods for estimating soil moisture over bare surfaces with Sentinel-1A dual-polarized data. IEEE *Journal of Selected Topics in Applied Earth Observations and Remote Sensing*, *16*: 4820–4832. https://doi. org/10.1109/JSTARS.2023.3275995.

Zan, F. De & Parizzi, A. (2013). A SAR interferometric model for soil moisture. *IEEE Xplore.* https://ieeexplore.ieee.org/abstract/document/6472061.

Zhu, L., Si, R., Shen, X., & Walker, J. P. (2022). An advanced change detection method for time-series soil moisture retrieval from Sentinel-1. *Remote Sensing of Environment*, *279*: 113137. https://doi.10.1016/ j.rse.2022.113137.

Zribi, M., Gorrab, A., & Baghdadi, N. (2014). A new soil roughness parameter for the modelling of radar backscattering over bare soil. *Remote Sensing of Environment*, *152*: 62–73. https://doi.org/10.1016/j. rse.2014.05.009.

Zribi, M., Muddu, S., Bousbih, S., Al Bitar, A., Tomer, S. K., Baghdadi, N., & Bandyopadhyay, S. (2019). Analysis of L-band SAR data for soil moisture estimations over agricultural areas in the tropics. *Remote Sensing*, *11* (9): 1122. https://doi.org/10.3390/rs11091122.